Human responses to upright tilt: a window on central autonomic integration. J Physiol. 1999;517:617-28.
17. Kawada T, Yanagiya Y, Uemura K, Miyamoto T, Zheng C, Li M, et al. Input-size dependence of the baroreflex neural arc transfer characteristics. Am J Physiol Heart Circ Physiol. 2003;284:H404-15.
18. Kashihara K, Takahashi Y, Chatani K, Kawada T, Zheng C, Li M, et al. Intravenous angiotensin II does not affect dynamic baroreflex characteristics of the neural or peripheral arc. Jpn J Physiol. 2003;53:135-43.
19. Kawada T, Miyamoto T, Miyoshi Y, Yamaguchi S, Tanabe Y, Kamiya A, et al. Sympathetic neural regulation of heart rate is robust against high plasma catecholamines. J Physiol Sci. 2006;56:235-45.
20. Minson J, Chalmers J, Kapoor V, Cain M, Caon A. Relative importance of sympathetic nerves and of circulating adrenaline and vasopressin in mediating hypertension after lesions of the caudal ventrolateral medulla in the rat. J Hypertens. 1986;4:273-81.
21. Kamiya A, Kawada T, Yamamoto K, Michikami D, Ariumi H, Miyamoto T, et al. Muscle sympathetic nerve activity averaged over 1 minute parallels renal and cardiac sympathetic nerve activity in response to a forced baroreceptor pressure change. Circulation. 2005;112:384-6.
22. Ichinose M, Saito M, Ogawa T, Hayashi K, Kondo N, Nishiyasu T. Modulation of control of muscle sympathetic nerve activity during orthostatic stress in humans. Am J Physiol Heart Circ Physiol. 2004;287:H2147-53.
23. Ichinose M, Saito M, Kitano A, Hayashi K, Kondo N, Nishiyasu T. Modulation of arterial baroreflex dynamic response during mild orthostatic stress in humans. J Physiol. 2004;557:321-30.

30th Annual International IEEE EMBS Conference
Vancouver, British Columbia, Canada, August 20-24, 2008

Modification of Autonomic Balance by Electrical Acupuncture does not Affect Baroreflex Dynamic Characteristics

Masaru Sugimachi, *Member, IEEE*, Toru Kawada,
Hiromi Yamamoto, Atsunori Kamiya,
Tadayoshi Miyamoto, and Kenji Sunagawa, *Member, IEEE*

Abstract— *Background:* We have demonstrated that modification of autonomic balance by electrical vagal stimulation delays progression of cardiac dysfunction and cardiac remodeling, and prolongs survival in rats with severe heart failure. We have also shown that we were able to modify autonomic balance by electrical acupuncture at the acupoint of Zusanli, potentially applicable for the treatment of heart failure. We examined the effect of the acupuncture on the dynamic characteristics of the baroreflex system to exclude the possible deleterious effect on orthostatic tolerance.

Method: In anesthetized 8 and 6 rabbits, we examined static and dynamic characteristics of baroreflex, respectively, with and without electrical acupuncture (1 Hz, 5 mA, and 5msec). Dynamic characteristics were examined by imposing pseudorandom binary changes in isolated carotid sinus pressure.

Results: With the stimulation condition to decrease arterial blood pressure and sympathetic nerve activity (resulted form decreased response range of neural arc), either of the dynamic characteristics of neural arc or those of peripheral arc did not change by electrical acupuncture at Zusanli.

Conclusion: We conclude that application of electrical acupuncture at Zusanli can suppress sympathetic nerve activity but does not affect the dynamic characteristics of the arterial baroreflex system, indicating no deleterious effect on orthostatic tolerance.

Manuscript received April 7, 2008. This work was supported in part by Health and Labour Sciences Research Grants (H19-nano-ippan-009, H15-physi-001) from the Ministry of Health Labour and Welfare of Japan, and by the Program for Promotion of Fundamental Studies in Health Science of the National Institute of Biomedical Innovation.

M. Sugimachi, D. Michikami, T. Kawada, H. Yamamoto, and A. Kamiya are with the National Cardiovascular Center Research Institute, Suita, Osaka 5658565, Japan (corresponding author Masaru Sugimachi to provide phone: +81-6-6833-512; fax: +81-6-6835-5403; e-mail: su91mach@ri.ncvc.go.jp).

D. Michikami is supported by a postdoctoral program by Japan Association for the Advancement of Medical Equipment.

T. Miyamoto is with Morinomiya University of Medical Sciences, Osaka 5590034 Japan. (e-mail: miyamoto@morinomiya-u.ac.jp).

K. Sunagawa is with Kyushu University Graduate School of Medical Sciences, Fukuoka 8128582 Japan. (e-mail: sunagawa@cardiol.med.kyushu-u.ac.jp).

I. INTRODUCTION

It is widely accepted that chronic heart failure involves not only abnormal structural and functional changes of heart and vessels themselves, but also abnormal changes in cardiovascular regulation. The fact that all successful cardiovascular drugs (ACE inhibitors, beta-adrenergic blockers, angiotensin receptor blockers, and aldosterone inhibitors) recently developed to treat heart failure are aimed at antagonizing neurohumoral activation has supported this.

We have shown that modification of autonomic balance by direct electrical vagal stimulation has inhibited cardiac remodeling, further deterioration of cardiac function, and improved survival in rat model of post-infarction severe chronic heart failure [1]. Because of the poor prognosis of chronic heart failure even with the use of combination of medical therapy, device-based therapy and the current state-of-art therapeutic modalities, such as cardiac transplantation, artificial heart, development of an additional therapeutic strategy attacking the abnormal cardiovascular regulation seems of great value to help still unsaved patients.

We have also shown in the last meeting that we were able to modify autonomic balance by electrical acupuncture at the acupoint of Zusanli, which is potentially applicable to treat heart failure. The less invasive nature of the acupuncture would greatly enhance its widespread use.

In this article, we have examined the effect of the acupuncture on the dynamic characteristics of the baroreflex system to ensure that there is no deleterious effect on orthostatic tolerance. The results indicated that electrical acupuncture is able to suppress sympathetic nerve activity but does not affect the dynamic characteristics of the arterial baroreflex system.

II. MODEL AND METHODS

A. Animal Experiments

We used 8 rabbits (Japanese White) to examine the effects of electrical acupuncture on open-loop static characteristics of baroreflex system. The effects of electrical acupuncture on open-loop dynamic characteristics were examined in other 6 rabbits.

978-1-4244-1815-2/08/$25.00 ©2008 IEEE.

In both protocols, rabbits were cared for in accordance with the Guiding Principles for the Care and Use of Animals in the Field of Physiological Sciences approved by the Physiological Society of Japan. These animals were anesthetized by a mixture of urethane (250 mg/ml) and α-chloralose (40 mg/ml) with an initial dose of 2 ml/kg (iv) and additional doses to maintain an appropriate level of anesthesia. Rabbits were mechanically ventilated with oxygen-enriched room air. Pancuronium bromide (0.1 mg/kg), a muscle relaxant was administered to prevent contaminating muscular activities.

A catheter-tipped micromanometer was inserted into a femoral artery to measure arterial blood pressure. After thoracotomy, we identified a left cardiac sympathetic nerve and the peripheral end was cut. Its efferent activity was recorded by a pair of stainless steel wire electrodes attached to the central end. We used silicone glue (Kwik-Sil, World Precision Instruments, Sarasota, FL) to fix the electrode, to provide insulation and to prevent the nerve from drying. We band-pass filtered the electrical signal at 150–1000 Hz and full-wave rectified, and low-pass filtered at a cutoff frequency of 30 Hz to quantify nerve activity.

To open the negative feedback loop, we isolated both carotid sinuses from the systemic circulation. We filled the isolated carotid sinuses with warmed physiological saline for longer preservation of baroreflex function. The blind-sac carotid sinuses were connected to a servo-controlled piston pump (model ET-126A, Labworks, Costa Mesa, CA) to control the pressure imposed on baroreceptors. Although being unphysiological and making baroreflex gain lower, it was necessary to cut bilateral vagal nerves and bilateral aortic depressor nerves to make baroreflex system fully open-loop condition.

Signals such as arterial blood pressure (AP), integrated sympathetic nerve activity (SNA), and carotid sinus pressure (CSP) were simultaneously digitized by a 12-bit analog-to-digital converter interfaced with a laboratory computer, and were stored on a hard disk for offline analysis. We used an arbitrary unit for nerve activity.

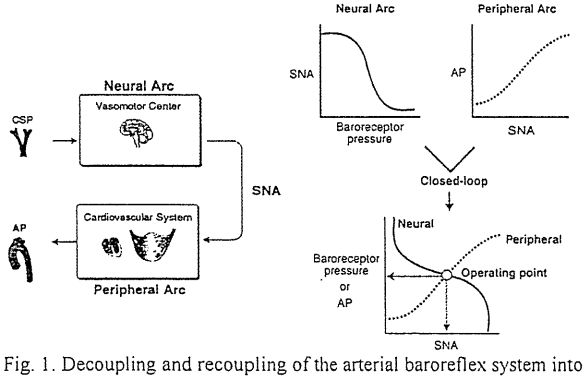

Fig. 1. Decoupling and recoupling of the arterial baroreflex system into neural arc and peripheral arc. CSP, carotid sinus pressure; AP, arterial blood pressure; SNA, sympathetic nerve activity.

B. Method to Identify Static Open-loop Characteristics of Baroreflex System

We have opened (see above) the total negative feedback loop of the arterial baroreflex system, and subdivided it into two subsystems. The two subsystems include the "neural arc" (which in turn includs baroreceptor and vasomotor center) and the "peripheral arc" (which in turn includes various sympathetic effectors). The neural arc corresponds to the controller and the peripheral arc corresponds to the plant of the baroreflex feedback system [2].

To quantify the static characteristics, we imposed stepwise change in CSP from 40 mmHg to 160mmHg with an increment of 20 mmHg. The particular CSP level was maintained for 60 seconds and the steady-state CSP, SNA, and AP were quantified by averaging the digitized values for the last 10 seconds.

We have characterized the neural arc by the relationship between CSP and SNA. We have characterized the peripheral arc by the relationship between SNA and AP. By recoupling these curves we can determine the operating point of the baroreflex system under the closed-loop condition by the intersection between the neural and peripheral arc curves.

C. Method to Identify Dynamic Open-loop Characteristics of Baroreflex System

We identified the dynamic characteristics of baroreflex, with or without electrical acupuncture. We imposed CSP changes around the respective closed-loop operating point with the amplitude of 20 mmHg according to a pseudorandom binary sequence.

The wideband nature of white noise input allows estimation of the wideband system dynamic properties. In addition, we ensemble-averaged the input power and cross power across multiple segments to reduce the statistical variance [3, 4].

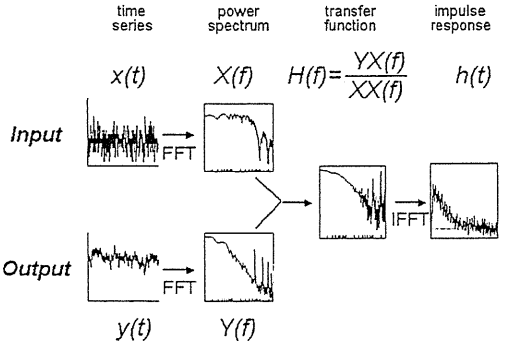

Fig. 2. Method to identify dynamic characteristics of a system. x(t), input signal; y(t), output signal; X(f) and Y(f), amplitude spectrum of x(t) and y(t), respectively; XX(f) and YX(f), ensemble-averaged input power spectrum and cross power (between input and output) spectrum, respectively; H(f), transfer function; h(t), impulse response.

We identified neural arc dynamic characteristics by analyzing CSP as input and SNA as output. We also identified peripheral arc dynamic characteristics by analyzing SNA as input and AP as output. Total baroreflex dynamic characteristics were obtained by analyzing CSP as input and AP as output.

In reference to Fig. 2, both input [x(t)] and output [y(t)] signals are divided into multiple segments. These data are subjected to frequency analysis using a fast Fourier transform (FFT) algorithm [X(f) and Y(f)]. The calculated input power and cross power (between input and output signals) are ensemble-averaged across segments to reduce variance [XX(f) and YX(f)]. Finally the transfer function [H(f)] is obtained by dividing the ensembled cross power by the ensembled input power. The impulse response [h(t)] is calculated by the inverse FFT of the transfer function.

D. *Electrical Acupuncture*

We have performed electrical acupuncture at Zusanli, i.e., the one-fifth point (from the knee) with the use of a pair of stainless steel wires (0.2 mm in diameter). The midpoint of the knee-ankle distance of approximately 30–35 mm served as the reference electrode. These needles were inserted to a depth of 10 mm in the skin and underlying muscle (the tibialis anterior muscle) [5].

The effects of Zusanli stimulation on baroreflex neural and peripheral arc characteristics were studied with the stimulation condition of 1 Hz, 5 mA, and 5msec. The stimulation condition is based on preliminary experiments.

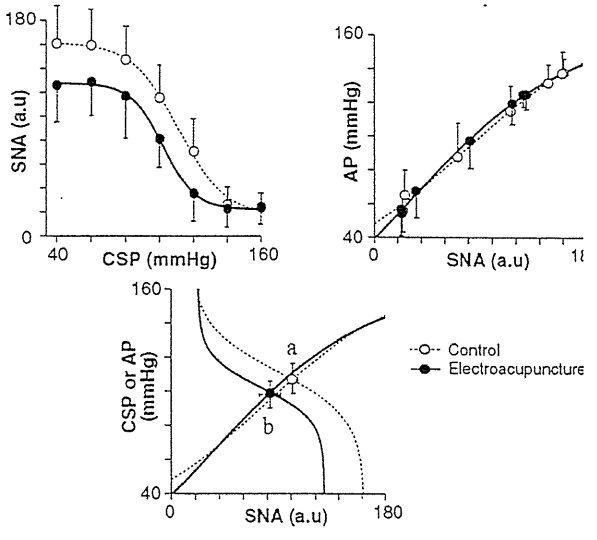

Fig. 3. Effect of electrical acupuncture on neural arc (top left) and peripheral arc (top right) static characteristics of arterial baroreflex, superimposed neural and peripheral arc curves (bottom). CSP, carotid sinus pressure; AP, arterial blood pressure; SNA, sympathetic nerve activity; solid line, with electrical acupuncture; dashed line, without electrical acupuncture, error bars, 1SD.

III. Results

A. *Effects on Static Characteristic*

The response range of SNA for the CSP change of 40-160 mmHg was obviously decreased with Zusanli stimulation (neural arc, Fig. 3 top left). The peripheral arc does not seem to change by Zusanli stimulation (Fig. 3 top right). These changes resulted in the decreased AP and SNA at the closed-loop operation point (Fig. 3 bottom).

B. *Effects on Dynamic Characteristic*

Fig. 4 exemplifies the time series of data obtained before and during pseudorandom changes in CSP. We imposed changes in CSP of ±20 mmHg around the respective closed-loop operating point.

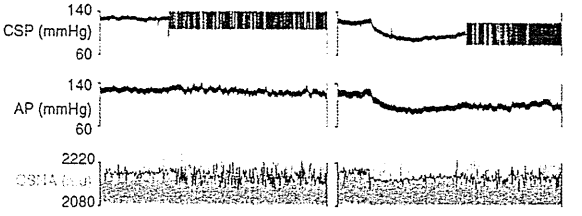

Fig. 4. An example of time series before and during changes in carotid sinus pressure according to pseudorandom binary sequence, with (right) and without (left) electrical acupuncture. CSP, carotid sinus pressure; AP, arterial blood pressure; CSNA, cardiac sympathetic nerve activity.

Changes in dynamic characteristics of neural arc, peripheral arc, and total loop by electrical acupuncture are shown in Fig. 5. As shown in the figure, transfer functions (dynamic characteristics) of neural arc, peripheral arc, and total loop were superimposable.

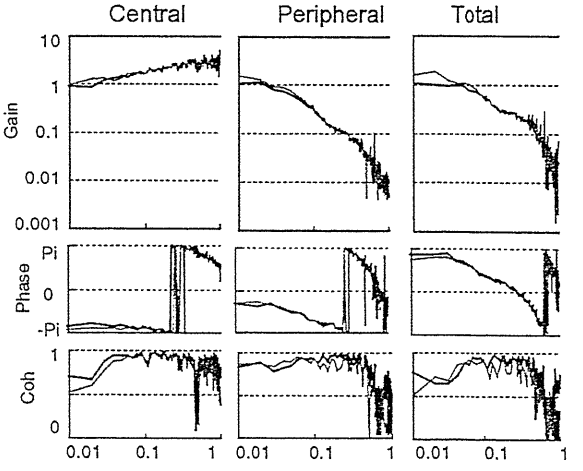

Fig. 5. Transfer functions (dynamic characteristics) of neural arc (left), peripheral arc (middle), and total loop (right) of baroreflex, with (gray) and without (black) electrical acupuncture. From top to bottom, gain, phase, and squared magnitude of coherence are shown.

IV. Discussion

We have repeatedly demonstrated that electrical vagal stimulation was successful in retarding further deterioration of cardiac function and progression of cardiac remodeling in rats with severe heart failure. This therapeutic method is also capable of prolonging survival in heart failure rats. These effects were believed to be mediated by the modification of autonomic balance.

Based on these results, several groups of investigators are developing an implantable vagal neurostimulators to apply this method for the human use; the invasive nature of the implantable device is likely to limit its widespread use, especially in relatively mild cases of heart failure.

A less invasive measure is definitely needed. To develop a less invasive method for modifying autonomic balance, we have examined the effect of Zusanli electrical stimulation. This method has been used to treat various diseases in oriental medicine.

To ensure these effects of traditional medicine, we have conducted animal experiments. The results have shown depressor and sympathetic neuroinhibitory (static) effect during Zusanli electrical stimulation. These effects are mediated by the changes in neural arc. We have also demonstrated that dynamic characteristics of baroreflex neural and peripheral arcs did not change by Zusanli electrical stimulation. We conclude that application of electrical acupuncture can suppress sympathetic nerve activity but does not affect the dynamic characteristics of the arterial baroreflex system, indicating no deleterious effect on orthostatic tolerance.

References

[1] M. Li, C. Zheng, T. Sato, T. Kawada, M. Sugimachi, K. Sunagawa. "Vagal nerve stimulation markedly improves long-term survival after chronic heart failure in rats." *Circulation.* Vol. 109, pp. 120-124, Jan. 2004.

[2] T. Sato, T. Kawada, M. Inagaki, T. Shishido, H. Takaki, M. Sugimachi, K. Sunagawa, "New analytic framework for understanding sympathetic baroreflex control of arterial pressure." *Am. J. Physiol. Heart Circ Physiol.* vol. 276, no. 6, pp. H2251-H2261, Jun. 1999.

[3] P. Z. Marmarelis and V. Z. Marmarelis, Analysis of Physiological Systems: The White-Noise Approach, New York, NY: Plenum, 1978.

[4] J. S. Bendat, and A. G. Piersol, Random Data: Analysis & Measurement Procedures, 3rd Ed., New York, NY: Wiley-Interscience, 2000

[5] D. Michikami, A. Kamiya, T. Kawada, M. Inagaki, T. Shishido, K. Yamamoto, H. Ariumi, S. Iwase, J. Sugenoya, K. Sunagawa, M. Sugimachi. "Short-term electroacupuncture at Zusanli resets the arterial baroreflex neural arc toward lower sympathetic nerve activity." *Am J Physiol Heart Circ Physiol.* vol. 291, pp. H318-H326, Jul. 2006.

Available online at www.sciencedirect.com
ScienceDirect
Biomaterials 29 (2008) 1307–1317
Biomaterials
www.elsevier.com/locate/biomaterials

Scaffolds from electrospun polyhydroxyalkanoate copolymers: Fabrication, characterization, bioabsorption and tissue response

Tang H. Ying [a,b], Daisuke Ishii [c], Atsushi Mahara [d], Sunao Murakami [d], Tetsuji Yamaoka [d], Kumar Sudesh [a,b], Razip Samian [b], Masahiro Fujita [a,*], Mizuo Maeda [a], Tadahisa Iwata [c,**]

[a] *Bioengineering Laboratory, RIKEN Institute, 2-1 Hirosawa, Wako-shi, Saitama 351-0198, Japan*
[b] *School of Biological Science, Universiti Sains Malaysia, 11800 Penang, Malaysia*
[c] *Department of Biomaterial Sciences, Graduate School of Agricultural and Life Sciences, The University of Tokyo, 1-1-1 Yayoi, Bunkyo-ku, Tokyo 113-8657, Japan*
[d] *Department of Biomedical Engineering, Advanced Medical Engineering Center, National Cardiovascular Center Research Institute, 5-7-1 Fujishirodai, Suita, Osaka 565-8565, Japan*

Received 10 September 2007; accepted 24 November 2007
Available online 21 December 2007

Abstract

Polyhydroxyalkanoate (PHA) copolymers of poly[(*R*)-3-hydroxybutyrate-*co*-5mol%-(*R*)-3-hydroxyhexanoate], poly[(*R*)-3-hydroxybutyrate-*co*-7mol%-4-hydroxybutyrate] and poly[(*R*)-3-hydroxybutyrate-*co*-97mol%-4-hydroxybutyrate] were electrospun to fabricate scaffolds with enhanced biocompatibility and bioabsorption. Subcutaneous implantation of the fibers in rats was performed to investigate their bioabsorption behavior and tissue response. The fibers before and after the *in vivo* experiments were characterized using gel permeation chromatography, scanning electron microscopy, X-ray diffraction and tensile test. Histological evaluation was also performed to determine the tissue response. The structures and properties of the electrospun PHA copolymers were compared with those of the electrospun poly[(*R*)-3-hydroxybutyrate]. The content and type of the second monomer and the diameter of fiber significantly influence the bioabsorption. The tissue response was found to improve with the high content of 4-hydroxybutyrate.

Keywords: Electrospun fiber; Polyhydroxyalkanoate; Tissue response; Bioabsorption

1. Introduction

In response to the growing demand in the field of tissue engineering, the number of polyhydroxyalkanoates (PHAs) currently under evaluation as biomaterial has expanded to five, that is, poly[(*R*)-3-hydroxybutyrate] [P(3HB)], poly (4-hydroxybutyrate) [P(4HB)], poly[(*R*)-3-hydroxybutyrate-*co*-4-hydroxybutyrate] [P(3HB-*co*-4HB)], poly[(*R*)-3-hydroxybutyrate-*co*-(*R*)-3-hydroxyvalerate] [P(3HB-*co*-3HV)] and poly[(*R*)-3-hydroxyoctanoate-*co*-(*R*)-3-hydroxyhexanoate] [P(3HO-*co*-3HHx)] [1]. To date, PHA and its composites are thought to have good potentials as emerging materials for medical devices such as sutures, bone plates, surgical mesh and cardiovascular patches, just to name a few [2]. A recent major breakthrough for PHA as a new class of biomaterial is the clearance obtained from the Food and Drug Administration of the United States of America for the use of P(4HB)-derived TephaFLEX® absorbable suture [3].

PHAs are a family of biopolyesters produced by numerous bacteria as intracellular carbon and energy compound under unfavorable growth conditions such as limitation of nitrogen, phosphorus, oxygen or magnesium in the presence of excess supply of carbon source [4–6]. PHAs are particularly attractive because they are bioabsorbable and biocompatible. The metabolism and excretion of some monomers incorporated into PHA

* Corresponding author. Tel.: +81 48 467 9312; fax: +81 48 462 4658.
** Corresponding author. Tel.: +81 3 5841 7888; fax: +81 3 5841 1304.
E-mail addresses: mfujita@riken.jp (M. Fujita), atiwata@mail.ecc.u-tokyo.ac.jp (T. Iwata).

0142-9612/$ - see front matter © 2007 Elsevier Ltd. All rights reserved.
doi:10.1016/j.biomaterials.2007.11.031

are well understood. For example, the monomeric component of P(3HB), (*R*)-3-hydroxybutanoic acid (3HB), is a ketone body present at concentrations of 3–10 mg per 100 mL blood in healthy adults [1,7]. The monomeric component of P(4HB), 4-hydroxybutanoic acid (4HB), can also be found widely distributed in the brain, kidney, heart, liver, lung and muscle of the mammalian body [8]. Furthermore, the hydroxyl acids released during PHA *in vivo* breakdown are found to be considerably less acidic and less inflammatory than many currently used synthetic absorbable polymers such as poly(lactic acid) (PLA) [9]. P(3HB) has, however, limited application due to its high brittleness, poor processability and slow degradation [10]. Therefore, researches in this field of interest had shown great progress over the past 20 years and it is now possible to design and synthesize various kinds of PHA (reviewed in Ref. [11]) to overcome the inferior properties of P(3HB).

New polymer processing approaches are in demand to create degradable porous scaffolds that can support the hierarchical structures of many tissues ranging between 0.1 and 1.0 mm [12]. Electrospinning has emerged as one of the methods offering simplicity and versatility in preparing such biomaterials [13]. Electrospun biomaterials facilitate better cell attachment and perfusion due to very high surface area-to-volume ratio and high porosity. Improved cellular response is also suggested because the morphology and architecture of electrospun structure are similar to those of some extracellular matrix (ECM) [14]. In addition, electrospinning may provide an alternative method to produce fibrous materials with improved mechanical properties compared to solid-walled equivalents [15].

Thus, in this study, we used electrospinning to develop scaffolds of fibrous PHA copolymers; P(3HB-*co*-5mol%-3HHx), P(3HB-*co*-7mol%-4HB) and P(3HB-*co*-97mol%-4HB) (Fig. 1), in aim of achieving enhanced biocompatibility, mechanical properties and bioabsorption. We also describe here the characterization and effects of sterilization on the physical properties of the electrospun PHA copolymers. Our study is the first to do a detailed comparison on the bioabsorption rate and the tissue response of electrospun PHA copolymers containing 3HB, 3HHx and 4HB monomers implanted subcutaneously in rat model.

2. Materials and methods

2.1. PHA synthesis

P(3HB-*co*-97mol%-4HB) was biosynthesized by *Delftia acidovorans* (formerly known as *Comamonas acidovorans*) using glucose and 1,4-butanediol as carbon sources, according to the method described in Ref. [16]. P(3HB-*co*-7mol%-4HB) was kindly provided by Dr. Toshihisa Tanaka of RIKEN Institute, Japan. The *in vitro* toxicity of P(3HB-*co*-4HB) derived from *D. acidovorans* has been determined recently [17]. P(3HB) and P(3HB-*co*-5mol%-3HHx) supplied by ICI Biopol and P&G, respectively, were purified before use. Briefly, the purification of the P(3HB) and P(3HB-*co*-5mol%-3HHx) was performed by dissolving the polymers in chloroform followed by precipitation in excess hexane and filtration.

2.2. Fabrication of fibrous implant and electrospinning

Each polymer solution of 1 wt% concentration was prepared by dissolving 100 mg of the polymer in 9900 mg of 1,1,1,3,3,3-hexafluoro-2-propanol (HFIP). Electrospinning was performed using Esprayer ES-2000 (Fuence, Co. Ltd., Japan). The polymer solution was placed in a 1-mL glass syringe with an inner needle diameter of 0.5 mm. The syringe was set vertically at the support of the electrospinning device and the solution was extruded at a constant rate of 40 μl min^{-1}. A positive voltage of 15 kV was applied at a distance of 20 cm between the needle tip and the copper collecting plate. The jet current was in the range of 38.3–38.7 μA and the collecting time was approximately 8 h. For effective collection of the electrospun fibers, a square fiber-collecting area (3 cm × 3 cm) was created on the copper plate by covering the rest of the plate with a non-conductive plastic. A sheet of aluminum foil was used to cover the collection area to ease the recovery of fibrous matrix from the copper plate. Each electrospun PHA scaffold was then cut into two different dimensions: 1 cm × 1 cm and 1 cm × 3 cm, respectively. All scaffolds were sterilized overnight with ethylene oxide (EtO) at 40 °C before implantation in rat.

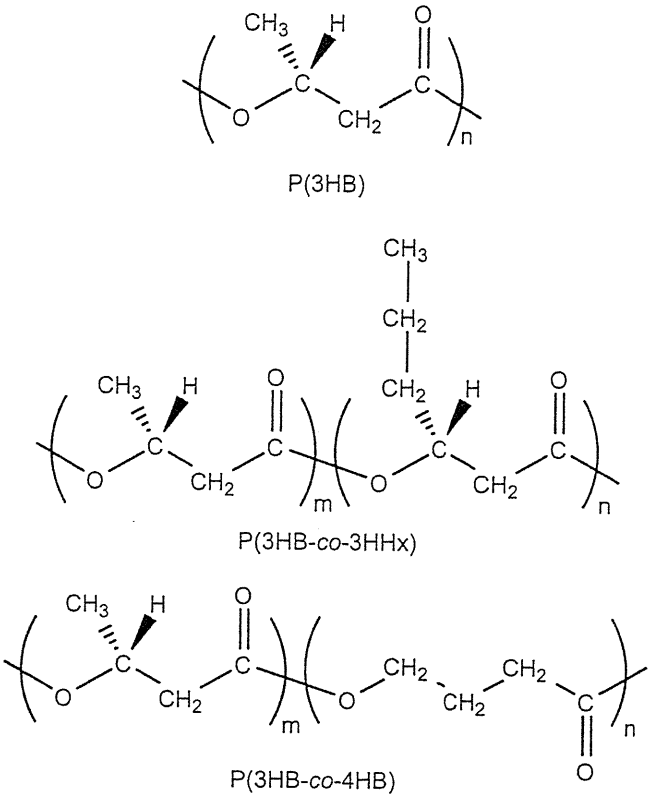

Fig. 1. Chemical structures of PHAs used in this study.

2.3. Subcutaneous implantation in rat and retrieval

Four 12-weeks-old male Wistar rats were used for implanting the PHA scaffolds; two for scaffolds measuring 1 cm × 1 cm while the remaining two for scaffolds measuring 1 cm × 3 cm. The animals were cared for in accordance with the Guiding Principles for the Care and Use of Animals in the Field of Physiological Sciences, approved by the Physiological Society of Japan. All experiment protocols had been reviewed and approved by the Animal Subjects Committee of the National Cardiovascular Center, Osaka, Japan. The rats were first injected with anesthetic before implanting the scaffolds. The 1 cm × 1 cm scaffolds were implanted subcutaneously at one side of the backbone while the 1 cm × 3 cm scaffolds were implanted subcutaneously at the backbone. The grouping of the rats was based on the duration of observation for 4 and 12 weeks. Upon explantation, the scaffolds measuring 1 cm × 1 cm were stored in 2.5% glutaraldehyde solution until further analysis by SEM. The retrieved 1 cm × 3 cm scaffolds were treated with 1.25 wt% trypsin to remove the surrounding tissues. They were then kept in tubes containing phosphate buffered saline (PBS) until further use.

2.4. Scanning electron microscopy

The PHA scaffolds were dehydrated in increasing concentrations of ethanol aqueous solutions containing 50%, 70%, 90%, 95%, 99.5% and 100%. They were then mounted on aluminum stumps and coated with gold in a sputtering device for 3 min at 5 mA. The scaffolds were observed with a scanning electron microscope (JSM-6330F, JEOL, Co. Ltd.) at an acceleration voltage of 5 kV and an emission current of 12 μA.

2.5. Wide-angle X-ray diffraction (WAXD)

Two-dimensional (2D) WAXD patterns of the electrospun PHA scaffolds were acquired using an X-ray diffractometer (RINT UltraX 18, Rigaku Japan) equipped with an imaging plate (BAS-SR 127, Fuji Film Co., Japan). Ni-filtered Cu–K_α radiation ($\lambda = 0.154$ nm) generated at 40 kV and 200 mA was collimated by a pinhole with a diameter of 1.0 mm. The distance from the scaffold to the imaging plate was 5 cm and the exposure time was 6 h. After converting the 2D images to 1D profile by circular-averaging, the crystallinity of the scaffolds was calculated from the ratio of the areas of crystalline reflections to the overall intensity in the range of $12° \leq 2\theta \leq 35°$ of the averaged 1D profile.

2.6. Tensile property

The non-sterilized scaffolds and the scaffolds before and after implantation were cut into 2 mm × 5 mm strips for tensile test. Tensile test on the scaffolds was carried out on a tensile testing machine (SHIMADZU EZTest) at a crosshead speed of 1 mm/min under ambient conditions. The thickness of each scaffold was measured before testing. Tensile properties were calculated from the stress–strain curves as means of two measurements.

2.7. Gel permeation chromatography (GPC) analysis

The molecular weight of the scaffolds was measured with gel permeation chromatography at 40 °C, using a Shimadzu 10A GPC system equipped with a 10A refractive index detector and Shodex K-806M and K-802 columns. Chloroform was used as the eluant at a flow rate of 1.0 ml min^{-1}. The calibration curve was prepared by using polystyrene standards with narrow polydispersity.

2.8. In vitro degradation evaluation

Each of the 1 cm × 3 cm sterilized scaffold was immersed in 10 mL phosphate buffered saline (PBS) at pH 7.4 in sterilized capped containers. These containers were then incubated at 37 °C without agitation. After 4 and 12 weeks, the scaffolds were recovered and characterized by SEM, tensile test, GPC and WAXD.

2.9. Histological observation

The surrounding tissues were excised together with the electrospun PHA scaffolds and fixed with 2.5% glutaraldehyde solution. A small piece of the tissue was then embedded in paraffin before subjecting it to microtome sectioning. Hematoxylin and eosin (HE) were used for staining the tissues. The tissue response to the scaffolds was evaluated from the coloration observed with a phase-contrast microscope.

3. Results and discussion

3.1. Morphological changes of electrospun PHA scaffolds

The retrieved electrospun PHA scaffolds showed various changes in appearances after subcutaneous implantation (Fig. 2). After 4 weeks, both the electrospun P(3HB) and P(3HB-*co*-5mol%-3HHx) remained in their initial form. The electrospun P(3HB-*co*-7mol%-4HB) was fragmented into large pieces while the electrospun P(3HB-*co*-97mol%-4HB) shrunk and became thinner. Even after 12 weeks, the electrospun P(3HB) showed no morphological change. However, significant changes were observed for the other three electrospun PHA copolymers. The degree of degradation increased in the order of P(3HB-*co*-5mol%-3HHx), P(3HB-*co*-7mol%-4HB), and (3HB-*co*-97mol%-4HB). The electrospun P(3HB-*co*-5mol%-3HHx) displayed crevices on its surface while the electrospun P(3HB-*co*-7mol%-4HB) was degraded into small fragments. Only a small piece of the electrospun P(3HB-*co*-97mol%-4HB) scaffold was retrieved, indicating enhanced bioabsorption of this 4HB-rich copolymer.

To have a better understanding on the progress of biodegradation at a fiber scale, SEM was used to observe the morphological changes of the fibers of all the electrospun PHA scaffolds. SEM revealed that all the as-spun scaffolds consist of randomly oriented fibers (Figs. 3 and 4). Further morphological feature is that the fibers fuse together. Namely, the electrospun fibers organize into a three-dimensional network. This is probably because the solvent (HFIP) evaporation was incomplete when the fibers were deposited on the collection plate. The width of the fiber between the junctions was quite uniform. The width decreased in the order of P(3HB) ≈ P(3HB-*co*-5mol%-3HHx) (520 nm) > P(3HB-*co*-97mol%-4HB) (220 nm) > P(3HB-*co*-7mol%-4HB) (190 nm). It has been reported that the width increases proportionally with the molecular weight of the polymer [18]. This is because higher degree of chain entanglement due to high molecular weight is assumed to make it harder for the electrostatic forces to pull, or extend individual chains [19]. Accordingly, the matrices of the electrospun P(3HB) and P(3HB-*co*-5mol%-3HHx) consisted of larger fibers compared to the electrospun P(3HB-*co*-97mol%-4HB) because of their high molecular weight (Table 1).

Interestingly, only the electrospun P(3HB-*co*-7mol%-4HB) formed fibers with irregular shapes with intermittent spindle-like beads on string (Fig. 4A). Possibly the formation of the beaded P(3HB-*co*-7mol%-4HB) fibers is the result of low net charge density. Previous studies have shown that higher net charge density favors the formation of bead-free fibers [20,21]. According to Ref. [20], the net charge density is inversely proportional to the mass of dry polymer (i.e. mass of scaffolds collected from electrospinning), if the other experimental conditions such as jet current, collecting time and polymer concentration are the same. The net charge density decreases in the order of P(3HB-*co*-5mol%-3HHx) (1058 C/l) > P(3HB) (1002 C/l) > P(3HB-*co*-97mol%-4HB) (778 C/l) > P(3HB-*co*-7mol%-4HB) (484 C/l). In this study, the P(3HB-*co*-7mol%-4HB) scaffold had the highest collected mass.

After sterilization, the morphologies observed for the electrospun P(3HB), P(3HB-*co*-5mol%-3HHx) and P(3HB-*co*-7ml%-4HB) remained unchanged (Figs. 3 and 4). The matrix of P(3HB-*co*-97mol%-4HB), however, became less porous

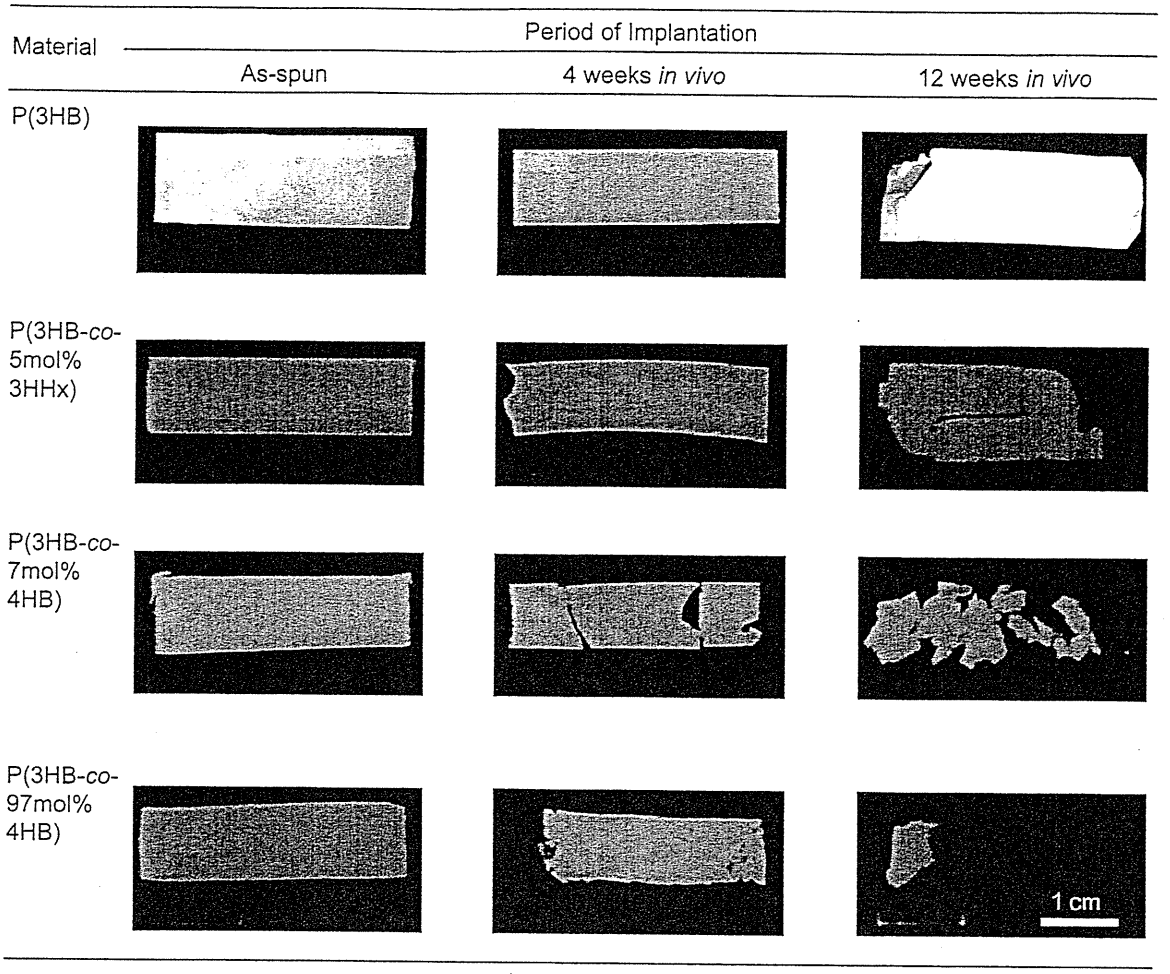

Fig.2. Physical appearance of the electrospun PHA scaffolds before and after 4 and 12 weeks of subcutaneous implantation in rat.

(Fig. 4B2). The temperature (40 °C) of the EtO sterilization is close to the melting temperature of P(3HB-*co*-97mol%-4HB) ($T_m = 47$ °C), and thus led to the fusing of some fibers to each other.

3.1.1. In vivo study

In SEM, only the remaining scaffolds that could be retrieved from rat after the *in vivo* experiments were observed. Nevertheless, such observations provided the information on the morphological changes by implantation. For the P(3HB) and P(3HB-*co*-5mol%-3HHx) scaffolds, no remarkable change in their appearances by implantation during the period investigated here was observed (Fig. 3). This result is in good agreement with the macro-scale observation, as shown in Fig. 2. On the other hand, the fibers of the copolymers with 4HB unit were influenced by the implantation. At 4 weeks of implantation, the fibers of P(3HB-*co*-97mol%-4HB) showed fragmentation (Fig. 4B3). After 12 weeks, surface erosion became more evident as the density of the fibers decreased remarkably due to fragmentation of the fibers to shorter segments. The progression of bioabsorption was also evidenced by the formation of pores on the surface of these fibers as indicated by the arrow in Fig. 4B4. These evidences indicate that the existence of 4HB monomer units enhances the degradability, or the bioabsorption of PHA.

After 4 and 12 weeks, the electrospun P(3HB-*co*-97mol%-4HB) fibers appeared to have swollen (Fig. 4B3 and B4). A slight decrease in the fiber density was also observed for the electrospun P(3HB-*co*-7mol%-4HB) (Fig. 4A4) at week 12. Previous studies have demonstrated that fibers of electrospun poly(D,L-lactic-*co*-glycolic acid), poly(D,L-lactic acid) and poly (butylene succinate) which were highly amorphous showed swelling after immersion in PBS [22–24]. Hence, it is possible that the swelling of the electrospun P(3HB-*co*-97mol%-4HB) fibers occurred due to the penetration of water into their amorphous regions.

3.1.2. In vitro study

SEM showed that there was no evidence of degradation on the surface of all the electrospun PHA scaffolds after 4 weeks of immersion in PBS (Figs. 3 and 4). All samples retrieved at 12 weeks also revealed that their structural integrities were maintained. This is because PHA hardly undergoes hydrolysis at pH value around neutrality. Similar to the observations for the *in vivo* study, the fibers of the electrospun P(3HB-*co*-97mol%-4HB) also demonstrated swelling.

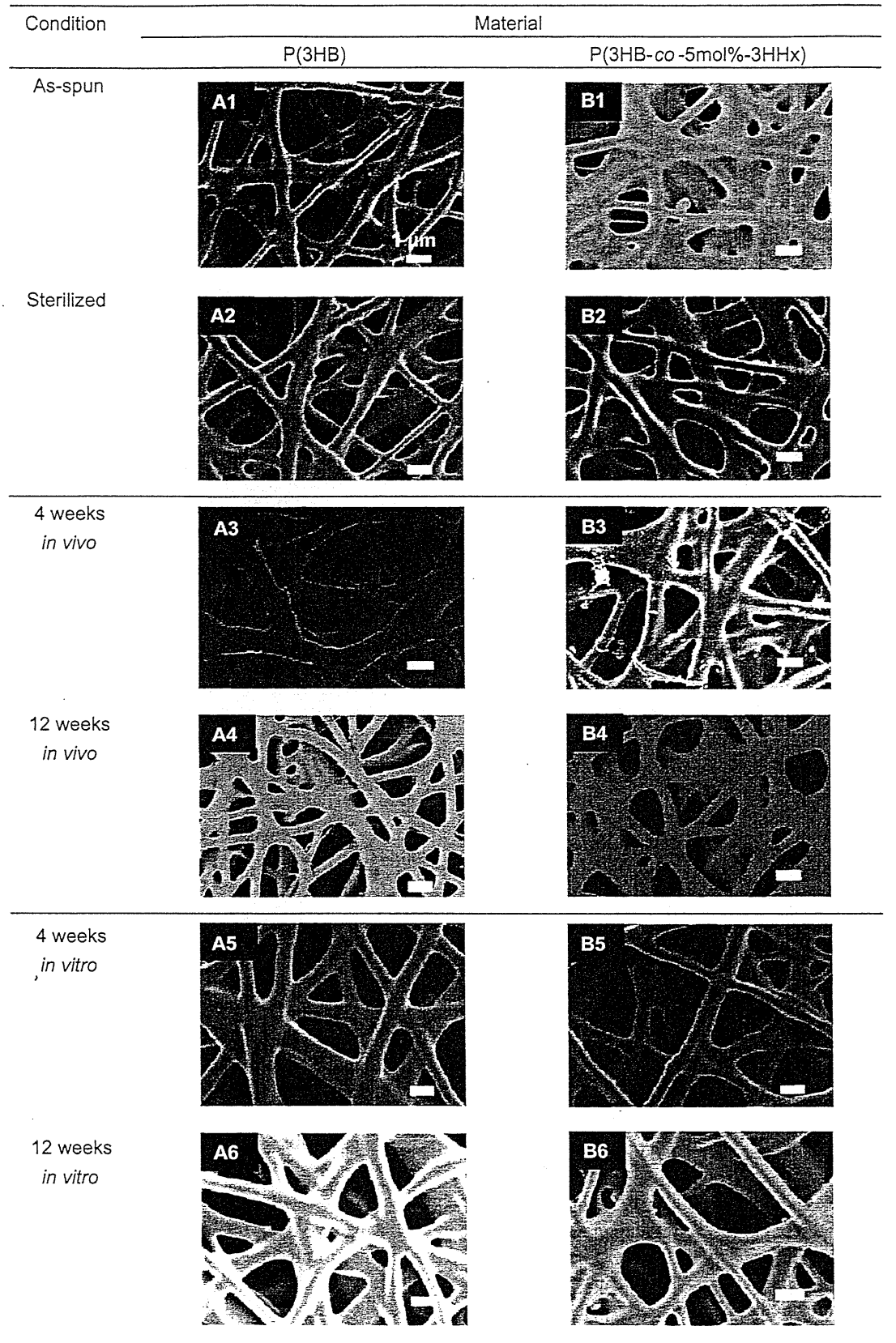

Fig. 3. SEM micrographs of the electrospun P(3HB) and P(3HB-*co*-5 mol%-3HHx) in various conditions.

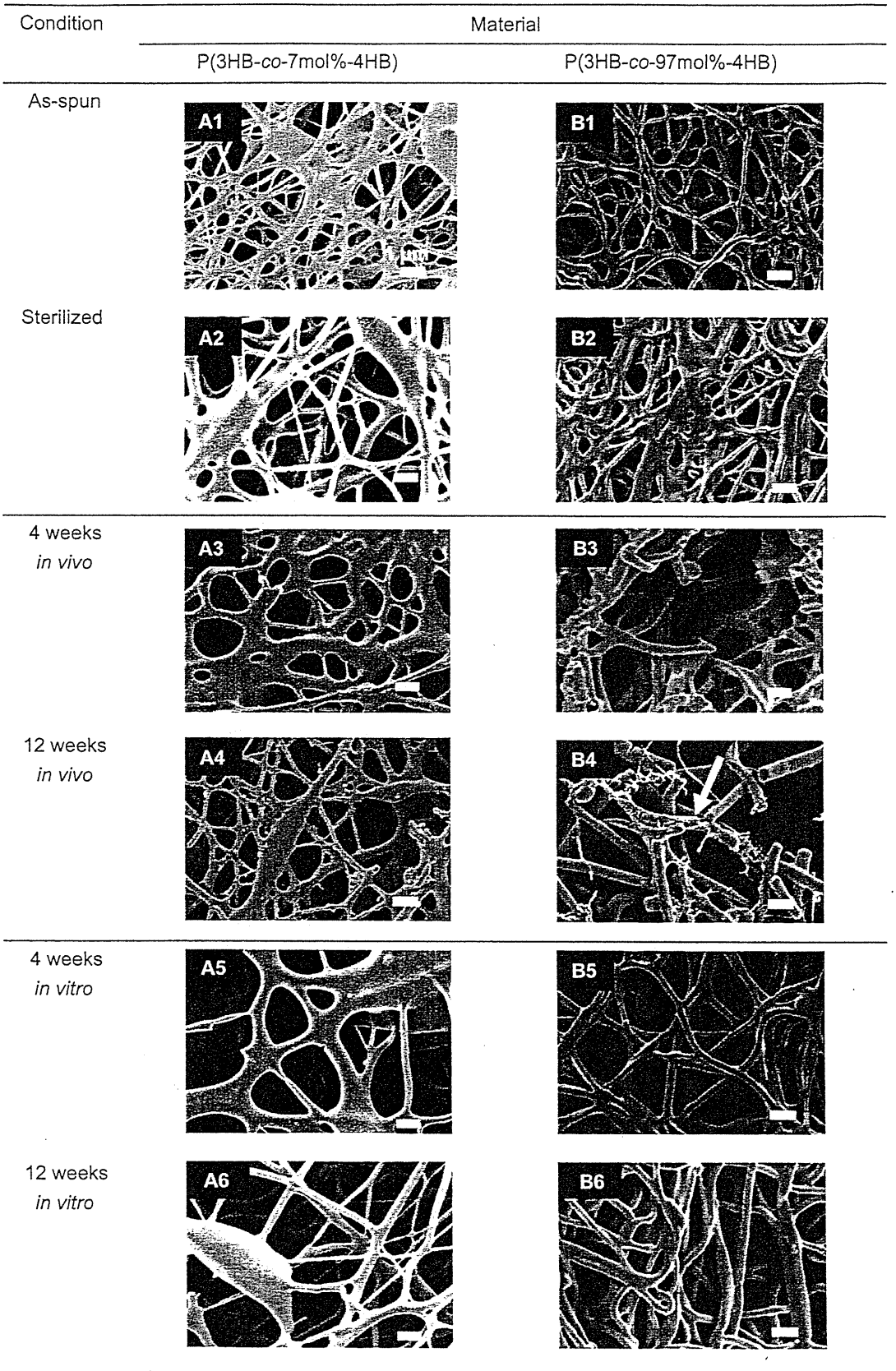

Fig. 4. SEM micrographs of the electrospun P(3HB-*co*-7 mol%-4HB) and P(3HB-*co*-97 mol%-4HB) in various conditions. The arrow shows the pores on the fiber.

Table 1
Molecular weight properties of the electrospun PHA scaffolds

Material	Condition	$M_w \times 10^5$	M_w/M_n
P(3HB)	As-spun	11	3.1
	Sterilized	9.1	3.3
	4 weeks *in vivo*	12	2.6
	4 weeks *in vitro*	11	2.6
	12 weeks *in vivo*	8.5	2.9
	12 weeks *in vitro*	17	3.3
P(3HB-*co*-5mol%-3HHx)	As-spun	13	3.6
	Sterilized	12	3.6
	4 weeks *in vivo*	12	3.1
	4 weeks *in vitro*	11	4.3
	12 weeks *in vivo*	11	3.3
	12 weeks *in vitro*	13	4.3
P(3HB-*co*-7mol%-4HB)	As-spun	7.0	3.0
	Sterilized	6.8	3.0
	4 weeks *in vivo*	6.4	2.6
	4 weeks *in vitro*	6.1	2.6
	12 weeks *in vivo*	3.9	2.7
	12 weeks *in vitro*	5.0	2.6
P(3HB-*co*-97mol%-4HB)	As-spun	1.7	1.5
	Sterilized	1.9	1.8
	4 weeks *in vivo*	1.0	1.6
	4 weeks *in vitro*	2.5	2.0
	12 weeks *in vivo*	1.2	2.0
	12 weeks *in vitro*	2.2	1.8

The *in vivo* and *in vitro* observations using SEM revealed that fibers with smaller diameter were more prone to fragmentation because of increased water contact due to large surface area. Thus, it can be concluded that surface erosion of the electrospun PHA scaffolds depends upon individual fiber dimensions and monomeric content.

3.2. Crystallinity

The WAXD profiles of the as-spun PHA scaffolds are displayed in Fig. 5. The profiles are the ones after subtraction of background. As shown in this figure, the crystalline reflections for the P(3HB) and the 3HB-rich copolymers could be indexed on the basis of P(3HB) α-form structure [25] while the crystalline phase of P(3HB-*co*-97mol%-4HB) fibers adopted the P(4HB) crystal structure [26]. From the 1D profiles, the crystallinity of as-spun, sterilized and scaffolds after *in vivo* and *in vitro* studies is estimated, according to the method described above. As shown in Fig. 6, the crystallinity of the as-spun PHA scaffolds increased in the order of P(3HB-*co*-97mol%-4HB) < P(3HB-*co*-5mol%-3HHx) ≈ P(3HB-*co*-7mol%-4HB) < P(3HB). This tendency is the same as the case of those bulk materials [27]. It has been reported that the crystallinity of P(4HB) homopolymer is much lower than that of P(3HB) homopolymer [28]. The slight lowering of the crystallinities of the 3HB-rich copolymers is due to the exclusion of second monomer unit from the crystalline lattice [29]. It is evident that the degradability of the scaffolds, as shown in Figs. 2 and 3, strongly depends on the crystallinity.

We confirmed that the EtO sterilization did not appear to have any effect on the crystallinities of all the electrospun

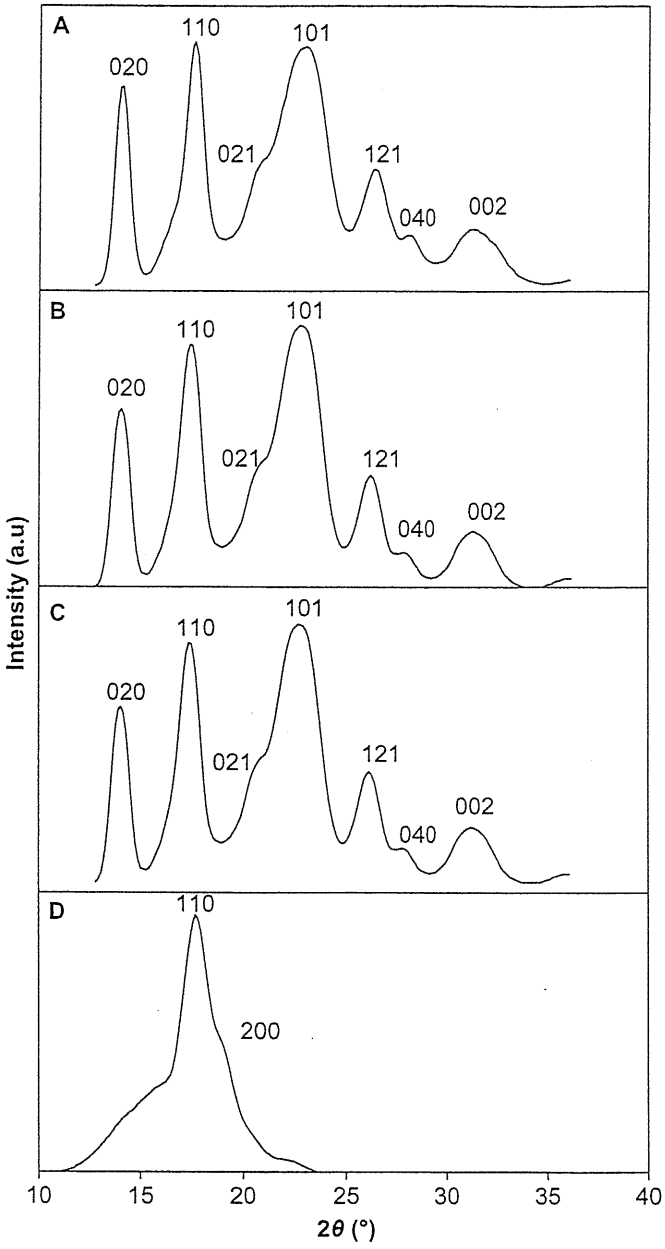

Fig. 5. Integrated 1D profiles from 2D WAXD patterns of as-spun: (A) P(3HB), (B) P(3HB-*co*-5 mol%-3HHx), (C) P(3HB-*co*-7 mol%-4HB) and (D) P(3HB-*co*-97 mol%-4HB).

PHA scaffolds. We described earlier that partial melting might occur during the sterilization of P(3HB-*co*-97mol%-4HB). Even if so, the crystallinity will surely recover after the sterilization. The crystallinities of the scaffolds after the *in vivo* and *in vitro* studies remained unchanged. But, it should be noted that the scaffolds for X-ray measurements are the retrieved or remained ones after *in vivo* and *in vitro* experiments. The crystallinity of the P(3HB-*co*-97mol%-4HB), which shows obvious bioabsorption or degradation in the macro-scale and SEM observations, also little changed even after implantation in rat. This means that the degradation of scaffolds progresses preferentially from the surface of the scaffolds or interface which contacts with the tissues of rat. It is deduced that some substance such as tissue enzymes facilitate the degradation [30].

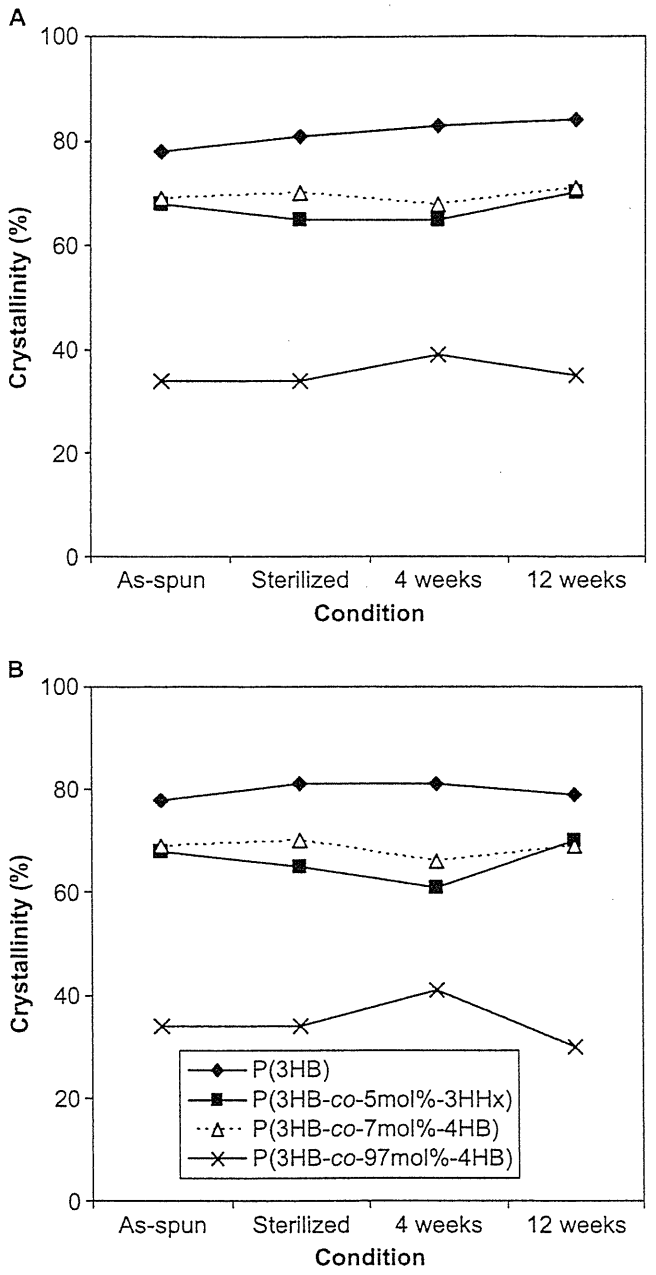

Fig. 6. Crystallinities of the electrospun PHA scaffolds in different conditions: (A) *in vivo* and (B) *in vitro*.

3.3. Molecular weight changes of electrospun PHA scaffolds

Table 1 summarizes the change in M_w and polydispersity index (M_w/M_n) for the as-spun scaffolds and scaffolds following sterilization, 4 and 12 weeks of *in vivo* and *in vitro* studies. After sterilization, all of the electrospun PHA scaffolds showed no significant differences in their molecular weight. Despite the large surface area of the fibers, PHA scaffolds remained intact in the *in vitro* study because they have higher resistance to hydrolysis in non-biological environment where specific enzymes are absent [27,31]. Furthermore, the immersion in PBS (pH 7.4) under sterile conditions up to only 12 weeks is short and the temperature is low for any significant hydrolysis to occur. The subcutaneous implantation, however, seems to cause decrease in the M_w of PHA copolymers with 4HB unit. At 4 weeks, bioabsorption was the most pronounced for the electrospun P(3HB-*co*-97mol%-4HB) with 47% loss M_w, while the M_w of P(3HB-*co*-7mol%-4HB) showed no decrease. Following longer implantation period, the electrospun P(3HB-*co*-7mol%-4HB) lost 43% of M_w. Unexpectedly, the electrospun P(3HB-*co*-97mol%-4HB) recorded only 37% of M_w loss after 12 weeks. It was confirmed that the number of main-chain carbon atom strongly influences the rate of hydrolysis.

3.4. Mechanical properties of electrospun PHA scaffolds

Table 2 summarizes the mechanical properties of electrospun PHA scaffolds obtained. The mechanical properties of all the as-spun scaffolds were comparable to those of human skin, and hence suggest they are mechanically stable in supporting regenerated tissues. The Young's modulus of the as-spun scaffolds increased in the order of P(3HB-*co*-97mol%-4HB) $\ll$ P(3HB-*co*-7mol%-4HB) $<$ P(3HB) $<$ P(3HB-*co*-5mol%-3HHx). Low Young's modulus, that is, high elasticity is a characteristic property in rubber-state amorphous polymers. Accordingly, this

Table 2
Mechanical properties of the PHA scaffolds

Material	Condition	Mechanical properties	
		Tensile strength (MPa)	Young's modulus (MPa)
P(3HB)	As-spun	17	223
	Sterilized	15	234
	4 weeks *in vivo*	12	182
	4 weeks *in vitro*	14	220
	12 weeks *in vivo*	15	152
	12 weeks *in vitro*	13	194
P(3HB-*co*-5mol%-3HHx)	As-spun	15	277
	Sterilized	12	272
	4 weeks *in vivo*	12	268
	4 weeks *in vitro*	13	208
	12 weeks *in vivo*	ND[b]	ND[b]
	12 weeks *in vitro*	15	230
P(3HB-*co*-7mol%-4HB)	As-spun	8	184
	Sterilized	8	139
	4 weeks *in vivo*	ND[b]	ND[b]
	4 weeks *in vitro*	8	163
	12 weeks *in vivo*	ND[b]	ND[b]
	12 weeks *in vitro*	9	110
P(3HB-*co*-97mol%-4HB)	As-spun	13	9
	Sterilized	15	16
	4 weeks *in vivo*	4	12
	4 weeks *in vitro*	11	14
	12 weeks *in vivo*	ND[b]	ND[b]
	12 weeks *in vitro*	14	16
Skin[a]		5–30	15–150

[a] Data obtained from Ref. [13].
[b] Not determined as the retrieved scaffolds from rat had cracks on the surface that prevented tensile test.

indicates that the P(3HB-*co*-97mol%-4HB) fibers are more amorphous than the other scaffolds, and this is consistent with the WAXD results. The distinct mechanical properties of the PHA could find different use as scaffolds for tissue engineering. For example, the 3HB-rich scaffolds which are more rigid could serve as preferential substrates for directional cell migration [32] while the compliant 4HB-rich scaffolds could be used to promote cell motility [33]. The EtO sterilization and the immersion in PBS buffer little affected the mechanical properties of all the scaffolds.

3.5. Histological observation

The histological sections of the electrospun PHA scaffolds at different period of subcutaneous implantation are shown in Fig. 7. Histological observations indicate that all the three electrospun copolymers elicited fairly mild tissue response relative to that of the electrospun P(3HB) throughout the course of study. After 4 weeks of implantation, some parts of the electrospun P(3HB-*co*-97mol%-4HB) bordering the interface were degraded as evidenced by the small fragments broken off from

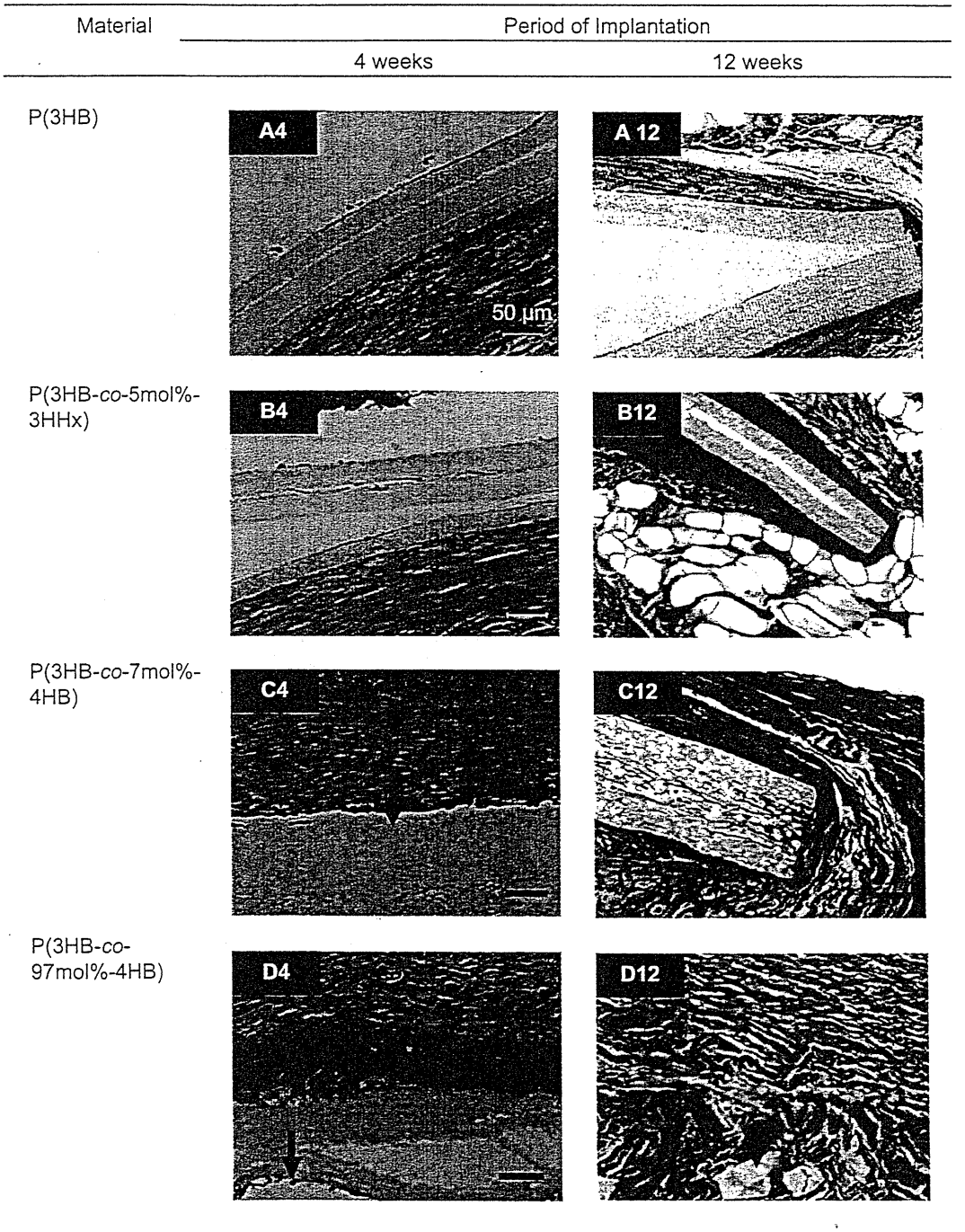

Fig. 7. Histological sections of the electrospun PHA scaffolds at different period of subcutaneous implantation. Arrows indicate the polymer surface.

the main scaffold (Fig. 7D4). More macrophages were found to be present along the interface connected to this copolymer in comparison to the electrospun P(3HB-*co*-7mol%-4HB) and P(3HB-*co*-5mol%-3HHx) (Fig. 7B4 and C4). This phenomenon is desirable during wound healing because the presence of macrophages is necessary for the regeneration of many cell types [34]. The presence of thin connective tissue surrounding the electrospun P(3HB-*co*-97mol%-4HB) was also observed.

The most promising finding was the tissue response after 12 weeks of implantation for the electrospun P(3HB-*co*-97mol%-4HB). No fibrous encapsulation was observed around the degraded copolymer and there was also a substantial drop in the number of inflammatory cells (Fig. 7D12). This observation is similar to a study done on the biocompatibility of P(4HB) implanted subcutaneously in rats by Martin et al. [35], that reported minimal inflammatory responses. In this study, the number of inflammatory cells surrounding the electrospun P(3HB-*co*-7mol%-4HB) and P(3HB-*co*-5mol%-3HHx) did not appear to have lessen. The muscle cells surrounding these two scaffolds appeared compact as a result of inflammatory reaction (Fig. 7B and C). After 12 weeks of implantation, the number of macrophages bordering the electrospun P(3HB) increased. Inflammation was obvious due to the compacted muscle cells surrounding the scaffold. The difference in tissue response to the electrospun P(3HB-*co*-97mol%-4HB) and the electrospun scaffolds with higher molar fraction of 3HB reflected their distinct physical properties. It has been reported that rigid polymer, such as P(3HB), elicit acute inflammatory reaction because it exerts a continuous mechanical stimulus to the surrounding tissues of the implants [36]. Although the tissue response to the electrospun P(3HB-*co*-7mol%-4HB) and electrospun P(3HB-*co*-5mol%-3HHx) was slightly more pronounced than that of the electrospun P(3HB-*co*-97mol%-4HB), the overall local tissue response to all three copolymers was found to be mild. The results have confirmed the biocompatibility of all three types of electrospun PHA copolymers.

3.6. Bioabsorption mechanism

The results from various analyses clearly demonstrated that the bioabsorption rate of the electrospun P(3HB-*co*-97mol%-4HB) was the fastest relative to the other two PHA copolymers. Three possible reasons for this observation are as follows: Firstly, the P(3HB-*co*-97mol%-4HB) with low crystallinity is more susceptible to bioabsorption as water and enzymes penetrate easier into the amorphous regions. Secondly, previous studies have established that macrophages are able to phagocytize PHA *in vitro* [37,38] and free radicals, acidic products or enzymes produced by these cells may also accelerate the degradation [39]. As seen in Fig. 7, the number of inflammatory cells was the most concentrated at the interface of electrospun P(3HB-*co*-97mol%-4HB) suggesting their active part in the bioabsorption process. Thirdly, possibly the enzymatic degradation by lipase also contributed to the rapid bioabsorption of the electrospun P(3HB-*co*-97mol%-4HB). PHA can be enzymatically degraded by PHA depolymerases, but there is no evidence to date that these are present *in vivo* [1]. P(4HB) was found to be also highly susceptible to lipase hydrolysis as opposed to P(3HB) [40]. Besides having good mechanical properties and biocompatibility, it is desirable for a medical implant to show good bioabsorption after its primary function has been fulfilled. The persistence of polymer at a wound healing site may lead to chronic inflammation as shown by the slowly degrading P(3HB) patches that elicited a long-term (greater than 2 years) macrophage response [41]. Hence the fast bioabsorption rates of the electrospun PHA containing 4HB have confirmed their potential in the application for medical implants.

4. Conclusion

In this study, electrospinning proved to be a simple and adaptable fabrication technique in producing constructs with dimensions approaching the native profile of ECM. Sterilization did not cause discoloration and damage to the PHA scaffolds. SEM revealed that both the *in vivo* and *in vitro* surface erosion of the electrospun PHA scaffolds progressed dependently on the individual fiber dimensions and monomeric contents. The mechanical properties demonstrated by all samples were comparable to those of human skin thus suggesting that their structures are able to provide sufficient biomechanical support. The electrospun scaffolds consisting of high 3HB content had higher degree of crystallinity and thus, they showed slower bioabsorption rate. GPC revealed that the *in vitro* degradation of the electrospun PHA scaffolds proceeded at a much slower rate in comparison to the *in vivo* bioabsorption. Histological evaluation showed that subcutaneous implantations of the electrospun PHA scaffolds were well tolerated *in vivo* as the tissue response continued to be very mild throughout the course of the study. Our results revealed that by changing the molar fraction of monomers in the PHA copolymers, it is possible to create tissue-engineering scaffolds that are tailor-made to meet the various needs in regenerating different cell type. The electrospun PHA copolymers proved to be promising biomaterials for scaffolds because of their biodegradability, flexible mechanical properties and excellent biocompatibility.

Acknowledgement

This work was supported by a Grant-in Aid for Scientific Research (B) from the Ministry of Education, Culture, Sports, Science and Technology (MEXT) of Japan (No.19350075) (to T. Iwata) and by a grant for Ecomolecular Science Research II provided by RIKEN Institute.

References

[1] Williams SF, Martin DP. Applications of PHAs in medicine and pharmacy. In: Steinbüchel A, editor. Series of biopolymers in 10 volumes, vol. 4. Wiley/VCY/Verlag; 2002. p. 91–121.

[2] Chen GQ, Wu Q. The application of polyhydroxyalkanoates as tissue engineering materials. Biomaterials 2005;26:6565–78.

[3] FDA clears first of its kind suture made using DNA technology. Available from: FDA News http://www.fda.gov/bbs/topics/NEWS/2007/NEW01560.html; 2007 February 12 [accessed 25.04.07].

[4] Anderson AJ, Dawes EA. Occurrence, metabolic role, and industrial uses of bacterial polyhydroxyalkanoates. Microbial Rev 1990;54:450–72.
[5] Doi Y. Microbial polyesters. New York: VCH; 1990.
[6] Kato M, Bao HJ, Kang CK, Fukui T, Doi Y. Production of a novel copolyester of 3-hydroxybutyric acid and medium-chain-length 3-hydroxyalkanoic acids by *Pseudomonas* sp. 61-3 from sugars. Appl Microbiol Biotechnol 1996;45:363–70.
[7] Hocking PJ, Marchessault RH. Biopolyesters. In: Griffin GJL, editor. Chemistry and technology of biodegradable polymers. London: Chapman & Hall; 1994. p. 48–96.
[8] Nelson T, Kaufman E, Kline E, Sokoloff L. The extraneural distribution of gammahydroxybutyrate. J Neurochem 1981;37:1345–88.
[9] Taylor MS, Daniels AU, Andriano KP, Heller J. Six absorbable polymers: *in vitro* acute toxicity of accumulated degradation products. J Appl Biomat 1994;5:151–7.
[10] Iwata T, Tsunoda K, Aoyagi Y, Kusaka S, Yonezawa N, Doi Y. Mechanical properties of uniaxially cold-drawn films of poly[(*R*)-3-hydroxybutyrate]. Polym Degrad Stab 2003:217–24.
[11] Sudesh K, Abe H, Doi Y. Synthesis, structure and properties of polyhydroxyalkanoates: biological polyesters. Prog Polym Sci 2000;25:1503–55.
[12] Griffith LG. Emerging design principles in biomaterials and scaffolds for tissue engineering. Ann N Y Acad Sci 2000;961:83–95.
[13] Zong X, Bien H, Chung CY, Yin L, Fang D, Hsiao BS, et al. Electrospun fine-textured scaffolds for heart tissue constructs. Biomaterials 2005;26: 5330–8.
[14] Li WJ, Laurencin CT, Caterson EJ, Tuan RS, Ko FK. Electrospun nanofibrous structure: a novel scaffold for tissue engineering. J Biomed Res 2002;60:613–21.
[15] Kim J, Reneker DH. Mechanical properties of composites using ultrafine electrospun fibers. Polym Composites 1999;20:124–31.
[16] Lee WH, Azizan MNM, Sudesh K. Effects of culture conditions on the composition of poly(3-hydroxybutyrate-*co*-4-hydroxybutyrate) synthesized by *Comamonas acidovorans*. Polym Degrad Stab 2004;84:129–34.
[17] Siew EL, Rajab NF, Osman A, Sudesh K, Inayat-Hussain SH. *In vitro* biocompatibility evaluation of poly(3-hydroxybutyrate-*co*-4-hydroxybutyrate) copolymer in fibroblast cells. J Biomed Res A 2007;81A:317–25.
[18] Dong H, Nyame V, Macdiarmid Jr AG, Jones WE. Polyaniline/poly(-methyl methacrylate) coaxial fibers: the fabrication and effects of the solution properties on the morphology of electrospun core fibers. J Polym Sci Part B: Polym Phys 2004;42:3934–42.
[19] Lyons J, Li C, Ko F. Melt-electrospinning part I: processing parameters and geometric properties. Polymer 2004;45:7597–603.
[20] Fong H, Chun I, Reneker DH. Beaded nanofibers formed during electrospinning. Polymer 1999;40:4585–92.
[21] Zuo W, Zhu M, Yang W, Yu H, Chen Y, Zhang Y. Experimental study on relationship between jet stability and formation of beaded fibers during electrospinning. Polym Eng Sci 2005;45:704–9.
[22] Zong X, Ran S, Kim KS, Fang D, Hsiao BS, Chu B. Structure and morphology changes during *in vitro* degradation of electrospun poly (glycolide-*co*-lactide nanofiber membrane. Biomacromolecules 2003;4: 416–23.
[23] Li WJ, Cooper Jr JA, Mauck RL, Tuan RS. Fabrication and characterization of six electrospun poly(α-hydroxyester)-based fibrous scaffolds for tissue engineering applications. Acta Biomaterialia 2006;2:377–85.
[24] Jeong EH, Im SS, Youk JH. Electrospinning and structural characterization of ultrafine poly(butylenes succinate) fibers. Polymer 2005;4: 9538–43.
[25] Yokouchi M, Chatani Y, Tadokoro H, Teranishi K, Tani H. Structural studies of polyesters: 5. Molecular and crystal structures of optically active and racemic poly (β-hydroxybutyrate). Polymer 1973;14: 267–72.
[26] Su F, Iwata T, Tanaka F, Doi Y. Crystal structure and enzymatic degradation of poly(4-hydroxybutyrate). Macromolecules 2003;36:6401–9.
[27] Doi Y, Kanesawa Y, Kawaguchi Y, Kunioka M. Biodegradation of microbial polyesters in the marine environment. Polym Degrad Stab 1992;32:173–7.
[28] Mitomo H, Hsieh WC, Nishiwaki K, Kasuya K, Doi Y. Poly(3-hydroxybutryate-co-4-hydroxybutyrate) produced by *Comamonas acidovorans*. Polymer 2001;42:3455–61.
[29] Di Lorenzo ML, Raimo M, Cascone E, Martuscelli E. Poly(3-hydroxybutyrate)-based copolymers and blends: influence of a second component on crystallization and thermal behavior. J Macromol Sci Phys 2001;40:639–67.
[30] Gogolewski S. Resorbable polymers for internal fixation. Clin Mater 1992;10:13–20.
[31] Marois Y, Zhang Z, Vert M, Deng X, Lenz R, Guidoin R. Mechanism and rate of degradation of polyhydroxyoctanoate films in aqueous media: a long term *in vitro* study. J Biomed Mater Res 2000;49:216–24.
[32] Lo CM, Wang HB, Dembo M, Wang YL. Cell movement is guided by the rigidity of the substrate. Biophys J 2000;79:144–52.
[33] Pelham RJ, Wang YL. Cell locomotion and focal adhesions are regulated by substrate flexibility. Proc Natl Acad Sci U S A 1997;94:13661–5.
[34] Rappolee DA, Mark D, Banda MJ, Werb Z. Wound macrophages express TGF-alpha and other growth factors *in vivo*: analysis by mRNA phenotyping. Science 1988;241:708.
[35] Martin DP, Skraly FA, Williams SF. Polyhydroxyalkanoate compositions having controlled degradation rats. PCT Patent Application No. WO 99/ 32536; 1999.
[36] Qu XH, Wu Q, Zhang KY, Chen GQ. *In vivo* studies of poly(3-hydroxybutyrate-*co*-3-hydroxyhexanoate) based polymers: biodegradation and tissue reactions. Biomaterials 2006;27:3540–8.
[37] Ali SAM, Doherty PJ, Williams DF. Molecular biointeractions of biomedial polymers with extracellular exudates and inflammatory cells and their effects on the biocompatibility *in vivo*. Biomaterials 1994; 15:779–85.
[38] Saad B, Neuenschwander P, Uhlschmid GK, Suter UW. New versatile, elastomeric, degradable polymeric materials for medicine. Intern J Biol Macromol 1999;25:293–301.
[39] Tracy MA, Ward KL, Firouzabadian L, Wang Y, Dong N, Qian R, et al. Factors affecting the degradation rate of poly(lactide-*co*-glycolide) microspheres *in vivo* and *in vitro*. Biomaterials 1999;20:1057–62.
[40] Mukai K, Doi Y, Sema Y, Tomita K. Substrate specificities in hydrolysis of polyhydroxyalkanoates by microbial esterases. Biotechnol Lett 1993;15:601–4.
[41] Malm T, Bowald S, Bylock A, Busch C, Saldeen T. Enlargement of the right ventricular outflow tract and the pulmonary artery with a new biodegradable patch in transanular position. Eur Surg Res 1994;26: 298–308.

TISSUE ENGINEERING: Part C
Volume 15, Number 00, 2009

DOI: 10.1089/ten.tec.2008.0483

Preservation of Porcine Hepatocytes in Three-Dimensional Bioreactor at Room Temperature Using Epigallocatechin-3-Gallate

Azizi Miskon, M.Eng.,[1–3] Tetsuji Yamaoka, Ph.D.,[1] Suong-Hyu Hyon, Ph.D.,[4] Makoto Kodama, Ph.D.,[3] and Hiroshi Uyama, Ph.D.[2]

A bioartificial liver (BAL) assist system employing a three-dimensional (3D) bioreactor has been studied as a temporary support in liver failure. In the present study, a novel preservation method of primary cultured porcine hepatocytes in monolayer and 3D culture systems was studied. Epigallocatechin-3-gallate (EGCG), which has recently been found to have various bioactivities, was selected as a key compound for hepatocyte preservation. Hepatocytes isolated from porcine liver using the collagenase perfusion method were pre-cultured for 6 days, preserved at room temperature in the presence of EGCG at various concentrations for 4 days, and post-cultured in normal medium for another 6 days. In the monolayer culture, only albumin production rate was fully recovered after preservation when EGCG concentration was high (0.25 mg/mL). In contrast, albumin production and ammonium metabolism in the 3D bioreactor under the same condition recovered to $72 \pm 16\%$ and $98 \pm 32\%$, respectively, of levels before preservation. These results indicate that hepatocytes can be preserved in the presence of 0.25 mg/mL of EGCG at room temperature, especially in a 3D culture system, which is promising technology for BAL preparation.

Introduction

VARIOUS CELL-BASED THERAPIES have been proposed and widely studied recently. Among them, hepatocyte-based treatments for fulminant or chronic hepatitis have been attracting great attention. Injection of hepatocytes isolated from unused donor livers and bioartificial liver (BAL) assist systems is used for treating acute liver failure and liver-based metabolic defects.[1–5] A large number of hepatocytes must be prepared for emergency care and for repeated treatment,[6] but because the isolation and reconstruction into a three-dimensional (3D) structure of the hepatocytes would take a long time and requires complex steps, metabolic activity rapidly decreases during the preparation process. We previously reported that the BAL system, using a radial flow bioreactor, needs at least 1.0×10^9 hepatocytes to maintain function.[7] Therefore, it is essential to preserve cells that maintain their functions in BALs. However, maintaining the specific functions of the hepatocytes using conventional cryopreservation is difficult.[8–16]

Various strategies to maintain cell functions have been proposed. Watts *et al.* and Mckay *et al.* reported that monolayer culture is superior to suspension culture in preserving hepatocytes.[17,18] Kakinoki *et al.* have succeeded in storing peripheral nerves for longer than 1 month using green tea polyphenol,[19] and Hyon *et al.* reported that green tea polyphenol also preserved the rat pancreatic islet for longer than 2 months.[20]

The green tea polyphenol is composed of epigallocatechin gallate, epicatechin gallate, epicatechin, and epigallocatechin, but the effect of each component on cell preservation is unknown. We focused on epigallocatechin-3-gallate (EGCG) because it is the main component of the green tea polyphenol and is well known to have a wide range of pharmacological activities, including antioxidant, anti-inflammatory, anti-atherogenic, and anti-thrombotic.[21–23] Recently, the effects of polyphenol on various diseases such as tissue ischemia,[24,25] neoplasm inflammation,[26,27] and arteriosclerosis[28,29] have been reported.

In the present study, we attempted to preserve primary cultured hepatocytes for a 3D BAL system. The effect of EGCG on hepatocyte preservation at room temperature was evaluated using monolayer culture. The preservation experiments in 3D BAL systems were also conducted in our

[1]Department of Biomedical Engineering, Advanced Medical Engineering Center, National Cardiovascular Center Research Institute, Osaka, Japan.
[2]Department of Chemical Engineering, Osaka University, Osaka, Japan.
[3]Graduate School of Life Science and Systems Engineering, Kyushu Institute of Technology, Kitakyushu City, Fukuoka, Japan.
[4]Institute for Frontier Medical Sciences, Kyoto University, Kyoto, Japan.

original BAL, which consisted of a perfusion-type bioreactor and a polytetrafluoroethylene (PTFE) non-woven fabric coated with the copolymer of poly (γ-methyl-L-glutamate) and poly urethane (PAU).[7]

Materials and Methods

Animals and hepatocytes

Mini pigs (male, 4–16 weeks) were purchased from Japan Farm LTD. (Kagoshima, Japan). Hepatocytes were isolated from the liver lobes (70–90 g) and used for a 2D monolayer culture experiment at the National Cardiovascular Center Research Institute (Osaka, Japan). The Animal Subjects Committee of the National Cardiovascular Center (Osaka, Japan) had reviewed and approved the experimental protocol.

A slaughtered pig (male, 7 weeks) was purchased from Kitakyushu Prefecture Edible Meat Center (Fukuoka, Japan). Hepatocytes were isolated from a liver lobe (103.4 g) and used for 3D BAL experiments at the Kyushu Institute of Technology (Fukuoka, Japan). The animal experiment was conducted in accordance with the Guiding Principles for the Care and Use of Animals in the Field of Physiological Science, approved by the Physiological Society of Japan.

Hepatocytes were isolated using the collagenase perfusion technique with modifications.[30,31] The liver was perfused with 1000 mL of calcium-free ethylenediaminetetraacetic acid (EDTA) buffer solution (0.15 M sodium chloride (NaCl), 5.63 mM calcium chloride (KCl), 0.02 M 4-(2-hydroxyethyl)-1-piperazineethanesulfonic acid (HEPES), 0.02 M sodium bicarbonate ($NaHCO_3$), and 0.99 mM EDTA disodium salt (EDTA·2Na; Wako, Ltd., Osaka, Japan), pH 7.4) at 80 mL/min and 37°C to remove the blood and then perfused with 500 mL of calcium-free buffer solution to rinse the EDTA·2Na, because EDTA·2Na reduces collagenase activity. After that, 500 mL of dispase solution (0.15 M NaCl, 5.63 mM KCl, 0.02 M HEPES, and 6.0×10^5 U Dispase; Gibco Co, Grand Island, NY) and then 500 mL os collagenase solution (0.15 M NaCl, 5.63 mM KCl, 0.02 M HEPES, 0.02 M $NaHCO_3$, 3.74 mM calcium chloride dihydrate ($CaCl_2{\cdot}2H_2O$), and 6.5×10^4 U collagenase (Wako, Ltd., Lot no. 06032W)) were perfused. The perfused liver was carefully minced with a scalpel blade, and the resulting crude homogenate was shaken in the presence of the last perfusate. The resulting cell suspension was filtered through nylon mesh with a 200-μm pore size and centrifuged at 600 rpm at 4°C for 2 min. The hepatocytes were washed with washing buffer with DNase (0.12 M NaCl, 6.2 mM KCl, 1.26 mM $CaCl_2{\cdot}2H_2O$, 0.49 mM magnesium chloride hexahydrate ($MgCl_2.6H_2O$). $6H_2O$, 0.41 mM magnesium sulfate heptahydrate $MgSO_4.7H_2O$, 10 mM HEPES, 1.0 g/L of bovine serum albumin (Wako, Ltd.), and 10 mg/L of DNase (Roche Diagnostics GmbH, Mannheim, Germany, Lot 13738000)) and with washing buffer (0.12 M NaCl, 6.2 mM KCl, 1.77 mM $CaCl_2{\cdot}2H_2O$, 0.02 M HEPES, and 1.0 g/L of bovine serum albumin (Wako, Ltd.)) twice.

Isolated hepatocytes were cultured in William's E medium with L-glutamate (Sigma-Adrich Inc., St. Louis, MO) supplemented with 10% (v/v) fetal bovine serum (Sigma-Adrich Inc., Lot no. 043K83032), 100 IU/L penicillin-streptomycin, 1.0×10^{-7} M insulin (Wako, Ltd.), 1.0×10^{-6} M dexamethasone (Wako, Ltd.), 25 μg/L epidermal growth factor (Sigma-Aldrich Inc.), and 1.5 mM L-ascorbic acid phosphate magnesium salt *n*-hydrate (Wako, Ltd.).

Cell culture

Static culture. Hepatocytes (1.0×10^6) were initially seeded on a 60-mm collagen type I–coated dish (Iwaki, Asahi

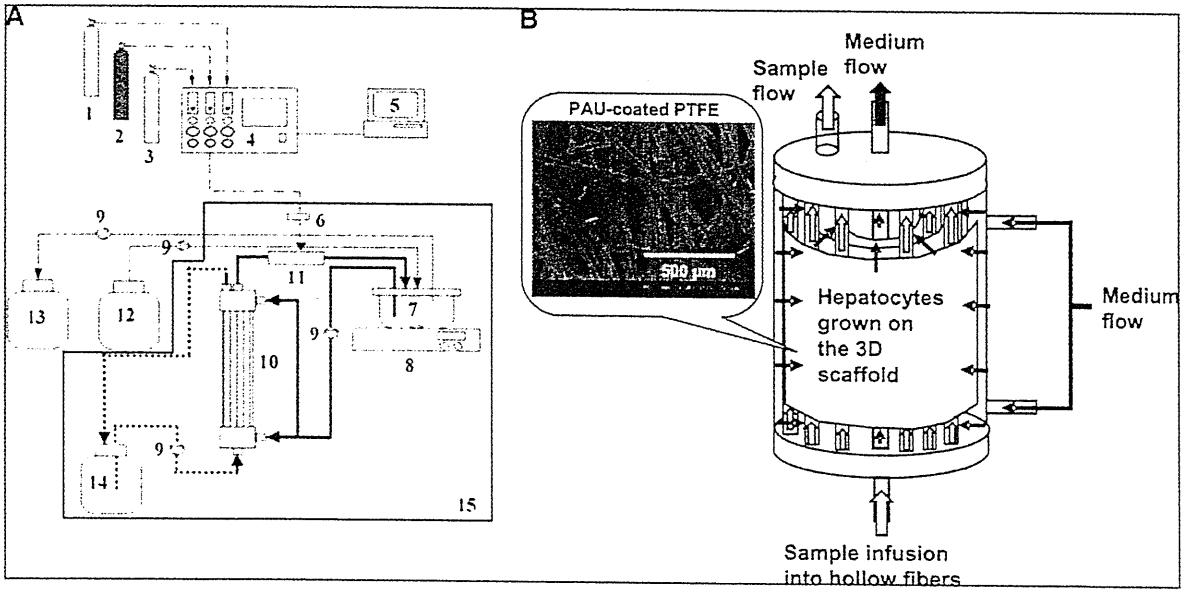

FIG. 1. (A) A schematic diagram of a bioartificial liver (BAL) (1) carbon dioxide cylinder, (2) oxygen cylinder, (3) air cylinder, (4) gas control equipment, (5) computer, (6) membrane filter, (7) conditioning vessel, (8) stirrer, (9) peristaltic pump, (10) radial flow bioreactor module, (11) silicone oxygenator module, (12) fresh medium tank, (13) spent medium tank, (14) plasma bottle, and (15) incubator. →: medium flow for hepatocytes culture. ····▶: Sample flow for ammonium metabolism evaluation. (B). Radial flow bioreactor module.

Glass Co., LTD, Tokyo, Japan) and incubated in a 5% carbon dioxide (CO_2)/air atmosphere at 37°C for 6 days. We started monitoring the hepatocyte functions on day 3 and continued for 4 more days (pre-preservation). After that, to preserve the hepatocytes, the given concentrations of EGCG (0, 0.25, 0.025, and 0.0025 mg/mL) were added to the culture medium and kept at room temperature for 4 days. CO_2 was not supplied during the preservation period. The preserved cells were properly washed with culture medium four times and cultured for 6 days in the normal medium (post-preservation). The medium was changed every 24 h.

The cell morphologies were observed at 3 days pre-preservation, on day 3 of the preservation period, and on 6 days in post-preservation using a Nikon TMS phase-contrast light microscope (Nikon, Tokyo, Japan). Images were taken using a Nikon CoolPix 990 digital camera (Nikon). The hepatocytes adhered in 2 days after seeding. Because of the high density of the seeded cells, the cells were in the confluent stage and do not proliferate.

Perfusion culture. Perfusion culture was performed in the radial flow bioreactor system that we reported previously.[7] In brief, hepatocyte suspension (2.0×10^9 cells in 50 mL) was inoculated into a conditioning vessel (Fig. 1A(7)) and perfused to a bioreactor module composed of a 3D scaffold made of PAU-coated PTFE non-woven fabric at the flow rate of 17 mL/min for 10 min. The suspension in the conditioning vessel was turbid because of the high density of inoculated cells before use (Supplementary data 1A). After 10 min of perfusion at 17 mL/min and 2 h of perfusion at 84.2 mL/min, the suspension became clear (Supplementary data 1B), and no cells were detected in the medium, indicating that the cell seeding efficiency was high and that almost all inoculated cells were adhered onto or entrapped in the non-woven scaffold.

The pH and oxygen concentration of the medium were fixed at 7.3 and 313 μM, respectively, using the pH and oxygen sensors of the conditioning vessel (Fig. 1A(7)). The gas controller equipment (Fig. 1A(4)) controlled air flow and carbon dioxide flow at 10 mL/min to control the pH. Meanwhile, the controller controlled oxygen at 50 mL/min to maintain the diluted oxygen rate.

We started monitoring the hepatocyte functions 24 h after inoculating the cells and continued for 4 days. The best

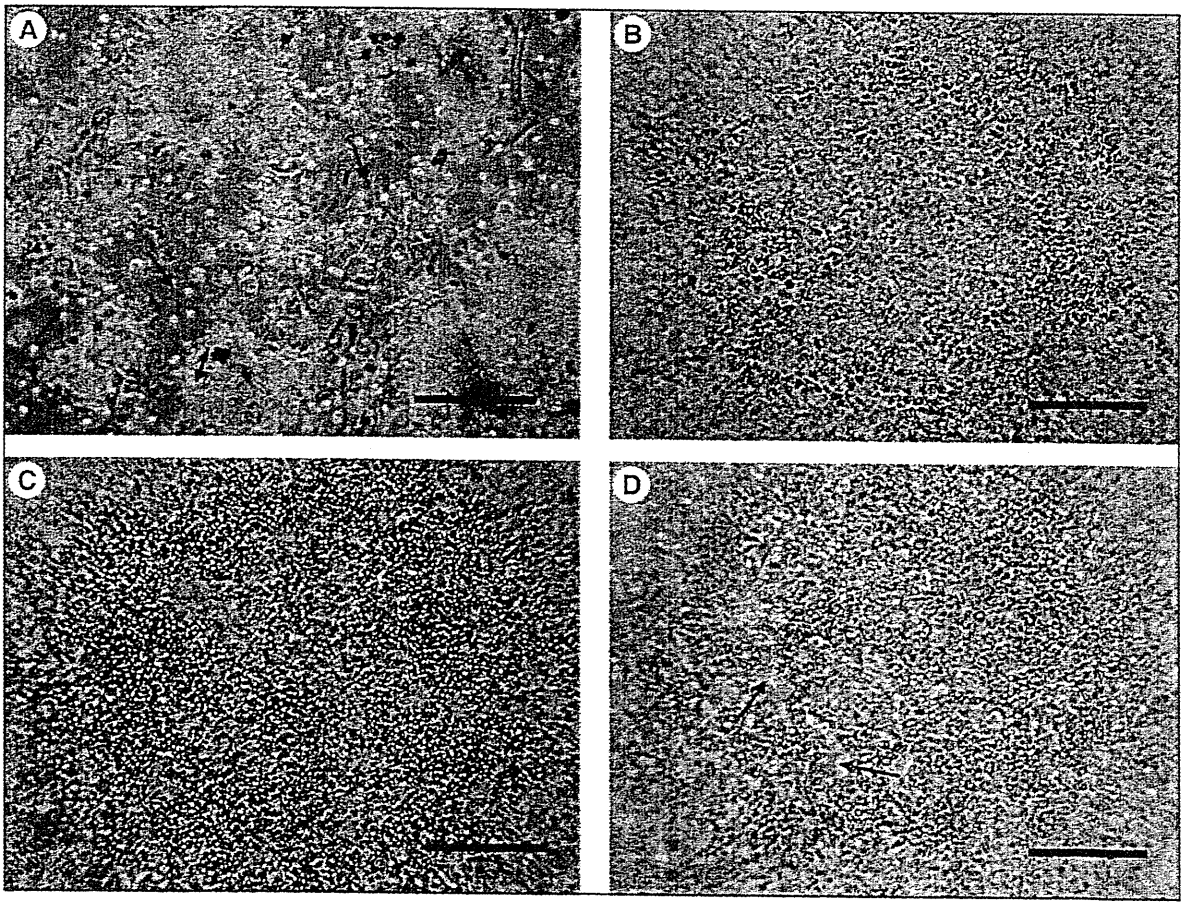

FIG. 2. Light microscopic images of porcine hepatocytes preserved for 3 days in (A) epigallocatechin-3-gallate (EGCG)-free medium or in EGCG-containing medium at the concentration of (B) 0.25-, (C) 0.025-, and (D) 0.0025-mg/mL EGCG. The arrows show the cells detaching from the dish. Bars represent 200 μm.

concentration of EGCG fixed in the monolayer culture system was applied to the 3D culture system and preserved at room temperature for 4 days. The medium perfusion and oxygen, air, and CO_2 supplies were stopped during the preservation period. The preserved cells were properly washed with 3 L of culture medium and cultured for 5 days in the normal medium. Medium exchange was performed every 24 h throughout the culture period.

Hepatocyte functions

Albumin production rate. One mL of medium was taken before and after the medium change in static and perfusion culture for measuring albumin production using enzyme-linked immunosorbent assay.[32] For the perfusion culture, the albumin concentration in the conditioning vessel and the plasma bottle were measured. Briefly, a 96-well plate was coated overnight with 1000-times-diluted goat anti-pig albumin antibody (Bethyl Lab, Inc., Montgomery, TX) at 4°C. The plate was washed four times with 1% (v/v) Tween 20 in phosphate buffered saline (PBS) (-), incubated with 0.01 g/mL block ace (Dainippon Sumitomo Pharma, Osaka, Japan) for 3 h at 37°C to block unspecific binding, and washed four times. Samples were added to the plate, incubated for 3 h at 37°C, and washed with 1% (v/v) Tween 20 in PBS (-) five times. The peroxidase-conjugated goat anti-pig albumin (Bethyl Lab, Inc., 15,000 times diluted) was added to each well and incubated for 2 h at 37°C. Afterward, the plate was washed, and the o-phenylenediamine (Wako, Ltd.) solution in 0.01% hydrogen peroxide (H_2O_2, 3 mg/mL) was added. The color reaction was stopped by adding 50 µL of 1.0 M sulfuric acid, and the ultraviolet absorbance was measured using a microplate reader at 490 nm. The albumin secretion is indicated as the amount in a dish and in a reactor per day (µg/dish per day, mg/reactor per day).

Ammonium metabolism rate

Static culture. To assess the ammonium metabolism of the hepatocytes, 1 mM ammonium chloride (NH_4Cl) was added to the medium, and the ammonium concentration was measured after 0, 3, and 6 h using the Amicheck meter (Arkray Factory Inc., Shiga, Japan). Ammonium metabolism rate defined as amount of decreased ammonium in a dish per hour (µmol/dish per h).

Perfusion culture. The plasma bottle (Fig. 1A(14)) of the 3D bioreactor system was filled with 300 mL of 1 mM NH_4Cl-containing medium, and the hepatocytes grown on the 3D scaffold (Fig. 1B) were perfused with this medium. The ammonium concentrations in the conditioning vessel and plasma bottle were measured after 0, 3, and 6 h using the Amicheck meter (Arkray Factory Inc.). The ammonium metabolism rate was expressed as µmol/reactor per hour.

Scanning electron micrography

Hepatocytes attached to the scaffold in the bioreactor were fixed with 2.5% glutaraldehyde, dehydrated with graded ethanol (50%, 60%, 70%, 80%, 90%, 95%, and 99.5%), and dried with tert-butyl alcohol (t-BuOH) freeze-drying (t-BuOH freeze dryer VFD-21; Vacuum Devices Co., Ltd., Ibaraki, Japan). The specimens were coated with palladium by sputtering (E-1030, Hitachi Co., Tokyo, Japan) and then observed using scanning electron microscopy (SEM; S-3000N, Hitachi Co.).

Histological study

The transverse section (2 µm thick) was taken from the construct in the bioreactor. The section was stained with hematoxylin and eosin (H&E) and azan to demonstrate

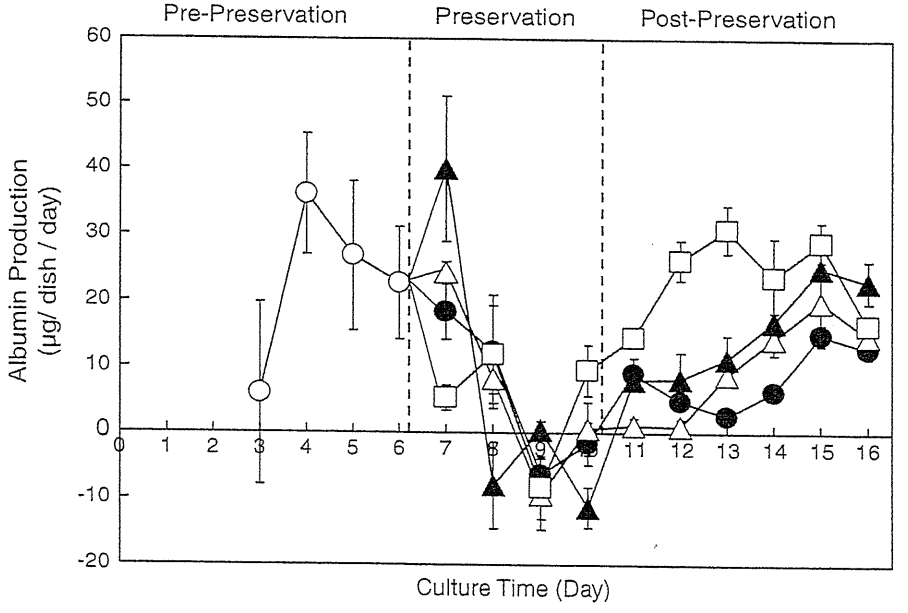

FIG. 3. Albumin production of monolayer-cultured hepatocytes during pre-preservation (○); preservation in epigallocatechin-3-gallate (EGCG)-free medium (●) and in 0.0025- (△), 0.025- (▲), and 0.25-mg/mL EGCG-containing medium (□).